Frontiers of Information Technology & Electronic Engineering
www.jzus.zju.edu.cn; engineering.cae.cn; www.springerlink.com
ISSN 2095-9184 (print); ISSN 2095-9230 (online)
E-mail: jzus@zju.edu.cn

Active fault-tolerant tracking control of a quadrotor with model uncertainties and actuator faults*

Yu-jiang ZHONG†1,2, Zhi-xiang LIU[2], You-min ZHANG†‡2, Wei ZHANG[1], Jun-yi ZUO[1]

[1]*School of Aeronautics, Northwestern Polytechnical University, Xi'an 710072, China*

[2]*Department of Mechanical, Industrial and Aerospace Engineering, Concordia University, Montreal H3G1M8, Canada*

†E-mail: yujiangzhong@hotmail.com; ymzhang@encs.concordia.ca

Received Sept. 15, 2018; Revision accepted Nov. 26, 2018; Crosschecked Jan. 8, 2019

Abstract: This paper presents a reliable active fault-tolerant tracking control system (AFTTCS) for actuator faults in a quadrotor unmanned aerial vehicle (QUAV). The proposed AFTTCS is designed based on a well-known model reference adaptive control (MRAC) framework that guarantees the global asymptotic stability of a QUAV system. To mitigate the negative impacts of model uncertainties and enhance system robustness, a radial basis function neural network is incorporated into the MRAC scheme for adaptively identifying the model uncertainties online and modifying the reference model. Meanwhile, actuator dynamics are considered to avoid undesirable performance degradation. Furthermore, a fault detection and diagnosis estimator is constructed to diagnose loss-of-control-effectiveness faults in actuators. Based on the fault information, a fault compensation term is added to the control law to compensate for the adverse effects of actuator faults. Simulation results show that the proposed AFTTCS enables the QUAV to track the desired reference commands in the absence/presence of actuator faults with satisfactory performance.

Key words: Model reference adaptive control; Neural network; Quadrotor; Fault-tolerant control; Fault detection and diagnosis

https://doi.org/10.1631/FITEE.1800570 **CLC number:** TP273

1 Introduction

During the last decade, quadrotor unmanned aerial vehicles (QUAVs) have attracted significant attention and experienced unprecedented growth in the civilian and military applications, owing to their unique capabilities in vertical takeoff and landing, and hovering at desired altitudes. This type of vehicle has been successfully employed in a variety of applications, such as aerial photography (Cheng, 2015), parcel delivery (Murray and Chu, 2015), forest fire surveillance (Yuan et al., 2015), and agriculture services (Zhang and Kovacs, 2012). In particular, because of the simple mechanical structures, affordable cost, and the abilities to fly in confined spaces, QUAVs have also become the ideal experimental platform for research laboratories, such as Aerospace Controls Lab at MIT (http://vertol.mit.edu.), Aerospace Robotics Lab at Stanford University (https://web.stanford.edu/group/arl/), Autonomous Systems Lab at ETH Zürich (http://www.asl.ethz.ch/the-lab.html), and Networked Autonomous Vehicles Lab at Concordia University (https://users.encs.concordia.ca/~ymzhang/UAVs). To complete various missions, an effective control system is indispensable in a QUAV. However, the QUAV is a nonlinear, underactuated, and

‡ Corresponding author

* Project supported by the National Natural Science Foundation of China (Nos. 61833013, 61573282, 61473227, and 11472222) and the Natural Sciences and Engineering Research Council of Canada

ORCID: You-min ZHANG, http://orcid.org/0000-0002-9731-5943

coupled system. It is a great challenge to design a high-performance trajectory tracking controller.

To track the desired trajectory accurately, some notable studies have been performed in recent years, such as linear quadratic regulators (Wang et al., 2016), fuzzy neural networks (Kayacan and Maslim, 2017), and terminal sliding mode control (Xiong and Zhang, 2017). In addition, various robust tracking control methods have been proposed to enhance the robustness of QUAV against model uncertainties and external disturbances, including fuzzy backstepping control (Yacef et al., 2016), guaranteed cost control (Xu et al., 2017), saturation control (Zou and Zhu, 2017), and continuous sliding mode control (Ríos et al., 2018). The aforementioned methods have been demonstrated to be effective for trajectory tracking in normal cases. However, they may not be effective when actuator faults occur, because these conventional controllers have insufficient fault-tolerant capabilities. In fact, actuators often fail to operate as expected owing to different types of malfunctions (Liu et al., 2017), which may significantly deteriorate system performance or even cause a QUAV crash. Therefore, actuator faults in the trajectory tracking problem cannot be ignored. To overcome such weaknesses, many fault-tolerant tracking control systems (FTTCSs) have been designed to achieve higher degrees of reliability and safety.

In general, the existing FTTCSs can be categorized into two types: passive FTTCS (PFTTCS) and active FTTCS (AFTTCS) (Zhang and Jiang, 2008). For PFTTCS, the fault-tolerant capability is attributable to the controller's robustness against presumed faults. Dydek et al. (2013) designed an adaptive PFTTCS using direct and indirect model reference adaptive control (MRAC), which provides increased robustness to actuator faults. Liu et al. (2016) developed a learning-based PFTTCS to counteract the negative effects of actuator faults and guarantee the tracking performance of a QUAV. Avram et al. (2018) proposed an adaptive fault-tolerant altitude and an attitude tracking method for a QUAV, which ensure a satisfactory tracking performance in the presence of multiple actuator faults. Mallavalli and Fekih (2018) employed an integral terminal sliding mode control approach to solve the problem of trajectory tracking for a QUAV with actuator faults and exogenous disturbances. Although tracking control in the presence of actuator faults has been addressed by the abovementioned PFTTCSs, these methods have limited fault-tolerant capabilities. Compared with PFTTCS, AFTTCS reacts to system failures actively via reconfiguring control actions based on the fault information. Thus, AFTTCS, to some extent, achieves better fault-tolerant performance. An observer-based AFTTCS was proposed to counteract the loss of control effectiveness in actuators (Hao and Xian, 2017), where an immersion and invariance observer was used to estimate the actuator fault and a unit quaternion representation was used to formulate the attitude of the tracking controller. Unfortunately, AFTTCS is limited to attitude tracking control, and the position tracking control is dismissed. In addition, little attention was paid to the AFTTCS for both position and attitude tracking control. The sliding mode control (SMC) technique was proposed for trajectory tracking, and an observer-based fault estimation scheme was designed to provide fault information for the SMC-based controller (Chen et al., 2015, 2016). However, owing to the high-frequency chattering characteristic of SMC, these two AFTTCSs are difficult to apply in engineering practice. Zhong et al. (2018a) proposed an AFTTCS to accommodate actuator faults and achieve an acceptable tracking performance, without consideration of actuator dynamics and model uncertainties.

Motived by the previous discussion, in this study, an active fault-tolerant tracking control system is designed to address trajectory tracking problems for a QUAV with model uncertainties and actuator faults. The basic idea is the integration of MRAC, radial basis function neural network (RBFNN), and fault detection and diagnosis (FDD) scheme in a stable and natural manner. The primary contributions of this paper can be summarized as: (1) A new AFTTCS is proposed for a QUAV against actuator faults with satisfactory performance and stability analysis is performed based on the Lyapunov stability theory; (2) In addition to actuator fault compensation, the proposed AFTTCS can achieve a satisfactory tracking performance when model uncertainties occur; (3) Actuator dynamics are considered to prevent actuators from exceeding their amplitudes and rate constraints, as well as to achieve a smooth actuator operation.

2 Problem formulation

As shown in Fig. 1, a QUAV is a multi-rotor aircraft with a simple geometric structure. Four motors are mounted on the midpoints of a rigid cross frame. The rotation of the fixed-pitch propellers produces thrusts for continuous QUAV flying. To balance the torques, two rotors (1 and 2) rotate in the clockwise direction, while the others (3 and 4) rotate in the opposite direction. The motions of a QUAV are controlled by changing the speed of each rotor. The pitch motion is achieved by conversely varying the speeds of the rotors (1 and 2). The roll motion is obtained by conversely varying the speeds of the rotors (3 and 4). Simultaneously adjusting the speeds of the four rotors will generate a vertical motion.

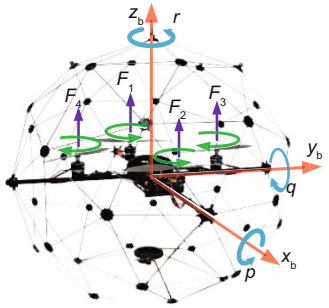

Fig. 1 Schematic of a quadrotor unmanned aerial vehicle

2.1 Dynamic model of a QUAV

The dynamics of a QUAV have been investigated by many researchers. As described in Xu and Ozguner (2006), the dynamic model of a QUAV with respect to the Earth-fixed coordinate system can be defined as

$$\begin{cases} \ddot{x} = (\cos\phi\sin\theta\cos\psi + \sin\phi\sin\psi)\frac{U_1}{m} - \frac{k_1}{m}\dot{x}, \\ \ddot{y} = (\cos\phi\sin\theta\sin\psi - \sin\phi\cos\psi)\frac{U_1}{m} - \frac{k_2}{m}\dot{y}, \\ \ddot{z} = (\cos\phi\cos\theta)\frac{U_1}{m} - g - \frac{k_3}{m}\dot{z}, \\ \ddot{\phi} = \frac{U_2}{I_x} - L\frac{k_4}{I_x}\dot{\phi}, \\ \ddot{\theta} = \frac{U_3}{I_y} - L\frac{k_5}{I_y}\dot{\theta}, \\ \ddot{\psi} = \frac{U_4}{I_z} - \frac{k_6}{I_z}\dot{\psi}, \end{cases} \tag{1}$$

with

$$\begin{cases} U_1 = F_1 + F_2 + F_3 + F_4, \\ U_2 = L(F_3 - F_4), \\ U_3 = L(F_1 - F_2), \\ U_4 = K_y(F_1 + F_2 - F_3 - F_4), \end{cases} \tag{2}$$

where the parameters are illustrated in Table 1.

Table 1 Notations used in this paper

Parameter	Definition
x, y, z	Coordinates in the inertial frame
ϕ, θ, ψ	Roll, pitch, yaw angles
I_x, I_y, I_z	Moment of inertia along x_b, y_b, z_b axes
k_i	Drag coefficient, $i = 1, 2, \ldots, 6$
m	Mass of a QUAV
g	Acceleration of gravity
U_1	Total lift force
U_2	Moment of roll
U_3	Moment of pitch
U_4	Moment of yaw
F_i	Thrust generated by the i^{th} motor, $i = 1, 2, 3, 4$
K_y	Thrust-to-moment scaling factor
L	Distance between the center of a QUAV and the rotor axis

To facilitate the design of AFTTCS, a simplified linear model must be chosen rather than a nonlinear model (1). Hence, the following assumption is required:

Assumption 1 It is assumed that the QUAV operates in a hovering condition ($U_1 \approx mg$). The pitch and roll motions are small such that $\sin\theta \approx \theta$ and $\sin\phi \approx \phi$. There is no yaw motion ($\psi = 0$) during the whole flight. Furthermore, the QUAV moves extremely slow, so the drag force can be neglected.

Based on Assumption 1, the simplified dynamic model can be obtained in the following form:

$$\begin{cases} \ddot{x} = \theta g, \\ \ddot{y} = -\phi g, \\ \ddot{z} = \frac{U_1}{m} - g, \\ \ddot{\phi} = \frac{U_2}{I_x}, \\ \ddot{\theta} = \frac{U_3}{I_y}, \\ \ddot{\psi} = \frac{U_4}{I_z}. \end{cases} \tag{3}$$

Denote $\boldsymbol{x}_\mathrm{p} = [x\ \dot{x}\ y\ \dot{y}\ z\ \dot{z}\ \phi\ \dot{\phi}\ \theta\ \dot{\theta}\ \psi\ \dot{\psi}]^\mathrm{T} \in \mathbb{R}^{n_\mathrm{p}}$ as the state vector, $\boldsymbol{u}_\mathrm{p} = [F_1\ F_2\ F_3\ F_4]^\mathrm{T} \in \mathbb{R}^p$ as the input vector, $\boldsymbol{y}_\mathrm{p} = [x\ y\ z\ \psi]^\mathrm{T} \in \mathbb{R}^m$ as the output vector; subsequently, the dynamic model (3) of a QUAV considering model uncertainties can be expressed in a state-space form:

$$\begin{cases} \dot{\boldsymbol{x}}_\mathrm{p}(t) = \boldsymbol{A}_\mathrm{p}\boldsymbol{x}_\mathrm{p}(t) + \boldsymbol{B}_\mathrm{p}\boldsymbol{u}_\mathrm{p}(t) + \boldsymbol{G}g, \\ \boldsymbol{y}_\mathrm{p}(t) = \boldsymbol{C}_\mathrm{p}\boldsymbol{x}_\mathrm{p}(t), \end{cases} \tag{4}$$

where $\boldsymbol{A}_\mathrm{p} = \boldsymbol{A}_{\mathrm{p}0} + \delta\boldsymbol{A}_\mathrm{p} \in \mathbb{R}^{n_\mathrm{p}\times n_\mathrm{p}}$, $\boldsymbol{B}_\mathrm{p} \in \mathbb{R}^{n_\mathrm{p}\times p}$, $\boldsymbol{C}_\mathrm{p} \in \mathbb{R}^{m\times n_\mathrm{p}}$ are the system matrices. $\boldsymbol{A}_{\mathrm{p}0} \in$

$\mathbb{R}^{n_\mathrm{p}\times n_\mathrm{p}}$ and $\delta\boldsymbol{A}_\mathrm{p}\in\mathbb{R}^{n_\mathrm{p}\times n_\mathrm{p}}$ represent the nominal system matrix and unknown model uncertainties, respectively.

Remark 1 The constant term $\boldsymbol{G}g$ is used to trim the quadrotor, so this term does not affect the controller design. For convenience, this term will be discarded hereinafter.

2.2 Actuator fault model

The actuators of a QUAV consist of four brushless motors and fixed-pitch propellers. When designing a controller for the QUAV, actuator dynamics are often neglected in most existing research. However, the system performance may be severely degraded because the controller cannot satisfy the physical constraints of the actuators. Therefore, actuator dynamics should be considered in the controller design procedure.

The thrust F_i generated by the i^{th} motor is related with the corresponding pulse-width-modulation (PWM) input u_i, which can be modeled by the following first-order linear transfer function (Liu et al., 2017):

$$F_i=K\frac{\omega}{s+\omega}u_i=\bar{K}u_i,\quad 0\le F_i\le\bar{F}_i,\tag{5}$$

where K denotes a positive gain, ω represents the motor bandwidth, and $\bar{F}_i$ is the maximum thrust provided by the i^{th} motor.

According to Eq. (5), the thrust variation rate can be derived as

$$F_{\mathrm{d}i}=\dot{F}_i=K\omega u_i-\omega F_i,\quad \underline{F}_{\mathrm{d}i}\le F_{\mathrm{d}i}\le\bar{F}_{\mathrm{d}i},\tag{6}$$

where $\underline{F}_{\mathrm{d}i}$ and $\bar{F}_{\mathrm{d}i}$ represent the lower bound and upper bound of $F_{\mathrm{d}i}$, respectively.

By considering actuator dynamics (5) and (6), the dynamic model (4) can be formulated as

$$\begin{cases}\dot{\boldsymbol{x}}_\mathrm{a}(t)=\boldsymbol{A}_\mathrm{a}\boldsymbol{x}_\mathrm{a}(t)+\boldsymbol{B}_\mathrm{a}\boldsymbol{u}(t),\\ \boldsymbol{y}_\mathrm{a}(t)=\boldsymbol{C}_\mathrm{a}\boldsymbol{x}_\mathrm{a}(t),\end{cases}\tag{7}$$

where $\boldsymbol{x}_\mathrm{a}=[\boldsymbol{x}_\mathrm{p}{}^\mathrm{T}\ \boldsymbol{u}_\mathrm{p}{}^\mathrm{T}]^\mathrm{T}\in\mathbb{R}^{n_\mathrm{p}+p}$ is the augmented system state vector, $\boldsymbol{u}=[u_1\ u_2\ u_3\ u_4]^\mathrm{T}\in\mathbb{R}^p$ is the control input vector, $\boldsymbol{A}_\mathrm{a}=\boldsymbol{A}_{\mathrm{a}0}+\delta\boldsymbol{A}_\mathrm{a}\in\mathbb{R}^{(n_\mathrm{p}+p)\times(n_\mathrm{p}+p)}$, $\boldsymbol{B}_\mathrm{a}=\begin{bmatrix}\bar{K}\boldsymbol{B}_\mathrm{p}\\ K\boldsymbol{\omega}\end{bmatrix}\in\mathbb{R}^{(n_\mathrm{p}+p)\times p}$, $\boldsymbol{C}_\mathrm{a}=[\boldsymbol{C}_\mathrm{p}\ \boldsymbol{0}]\in\mathbb{R}^{m\times(n_\mathrm{p}+p)}$ are the augmented system matrices. $\boldsymbol{A}_{\mathrm{a}0}=\begin{bmatrix}\boldsymbol{A}_{\mathrm{p}0}&\boldsymbol{0}\\ \boldsymbol{0}&-\boldsymbol{\omega}\end{bmatrix}\in\mathbb{R}^{(n_\mathrm{p}+p)\times(n_\mathrm{p}+p)}$ and $\delta\boldsymbol{A}_\mathrm{a}\in\mathbb{R}^{(n_\mathrm{p}+p)\times(n_\mathrm{p}+p)}$ denote the augmented nominal system matrix and unknown model uncertainties, respectively.

As a typical type of actuator fault, the partial loss of control effectiveness (LOE) in an actuator is discussed herein. The LOE fault is characterized by a reduction in the control command because of an unexpected damage to the propellers or motors. In other words, the control command from the controller cannot be transformed into the desired manipulated variables entirely (Zhang and Jiang, 2002). By introducing an LOE factor $\gamma_i, i=1,2,\dots,p$, an LOE fault can be modeled as

$$u_i^\mathrm{f}=(1-\gamma_i)u_i,\ 0\le\gamma_i\le 1,\tag{8}$$

where $\gamma_i=0$ or $\gamma_i=1$ represents that the i^{th} actuator is completely healthy or fails, respectively, and $0<\gamma_i<1$ denotes the partial LOE in the i^{th} actuator.

Using Eqs. (7) and (8), the dynamic model of a QUAV considering actuator faults and model uncertainties can be represented as

$$\dot{\boldsymbol{x}}_\mathrm{a}(t)=\boldsymbol{A}_\mathrm{a}\boldsymbol{x}_\mathrm{a}(t)+\boldsymbol{B}_\mathrm{a}(\boldsymbol{I}-\boldsymbol{\Gamma})\boldsymbol{u}(t),\tag{9}$$

or in a compact form, as

$$\dot{\boldsymbol{x}}_\mathrm{a}(t)=\boldsymbol{A}_\mathrm{a}\boldsymbol{x}_\mathrm{a}(t)+\boldsymbol{B}_\mathrm{a}\boldsymbol{u}_\mathrm{a}(t)+\boldsymbol{E}_\mathrm{a}\boldsymbol{\gamma}(t),\tag{10}$$

where $\boldsymbol{\Gamma}=\mathrm{diag}\,(\gamma_1,\gamma_2,\dots,\gamma_p)$, $\boldsymbol{\gamma}=[\gamma_1\gamma_2\dots\gamma_p]^\mathrm{T}$, $\boldsymbol{E}_a=-\boldsymbol{B}_a\boldsymbol{U}$, and $\boldsymbol{U}=\mathrm{diag}\,(u_1,u_2,\dots,u_p)$.

The above equation can be represented in another form:

$$\dot{\boldsymbol{x}}_\mathrm{a}(t)=\boldsymbol{A}_\mathrm{a}\boldsymbol{x}_\mathrm{a}(t)+\boldsymbol{B}_\mathrm{a}\boldsymbol{u}_\mathrm{a}(t)+\underline{\boldsymbol{E}}_\mathrm{a}\boldsymbol{f}(t),\tag{11}$$

where $\underline{\boldsymbol{E}}_\mathrm{a}=-\boldsymbol{B}_\mathrm{a}$, $\boldsymbol{f}(t)=\boldsymbol{U}\boldsymbol{\gamma}(t)$.

3 Active fault-tolerant tracking control system design

3.1 Fault detection and diagnosis scheme

Accurate fault information is important in the design of an AFTTCS. The FDD scheme is first presented herein. Because the proposed FDD scheme is designed based on a discrete filter, it is essential to obtain a discrete-time dynamic model of the QUAV. Using the zero-order holder with sampling at 50 Hz, the dynamic model (10) can be discretized as

$$\begin{cases}\boldsymbol{x}_{k+1}=\boldsymbol{A}_k\boldsymbol{x}_k+\boldsymbol{B}_k\boldsymbol{u}_k+\boldsymbol{E}_k\boldsymbol{\gamma}_k+\boldsymbol{\omega}_k^x,\\ \boldsymbol{y}_k=\boldsymbol{C}_k\boldsymbol{x}_k+\boldsymbol{v}_k,\end{cases}\tag{12}$$

where $\boldsymbol{\omega}_k^x$ and $\boldsymbol{v}_k$ are uncorrelated white Gaussian noise sequences with covariances $\boldsymbol{Q}_k^x$ and $\boldsymbol{R}_k$, respectively.

In general, the true value of $\boldsymbol{\gamma}_k$ is unknown; thus, the LOE factor is modeled as a stochastic process:

$$\boldsymbol{\gamma}_{k+1}=\boldsymbol{\gamma}_k+\boldsymbol{w}_k^{\gamma}, \tag{13}$$

where $\boldsymbol{w}_k^{\gamma}$ denotes the zero-mean white noise sequence with covariance $\boldsymbol{Q}_k^{\gamma}$.

To perform fault detection and diagnosis, an adaptive two-stage kalman filter (ATSKF) is applied to identify the LOE factor (Wu et al., 2000; Zhang and Jiang, 2002). ATSKF consists of two parallel subfilters: one is used to estimate the fault parameter and the other is used to estimate the system state. Therefore, ATSKF can simultaneously provide a minimum variance estimation of the fault and state.

The fault parameter subfilter is as follows:

$$\widehat{\boldsymbol{\gamma}}_{k+1|k}=\widehat{\boldsymbol{\gamma}}_{k|k}, \tag{14}$$

$$\boldsymbol{P}_{k+1|k}^{\gamma}=\sum_{i=1}^{m}\frac{1}{\rho_k^i}\boldsymbol{e}_k^i\alpha_{k|k}^i(\boldsymbol{e}_k^i)^{\mathrm{T}}+\boldsymbol{Q}_k^{\gamma}, \tag{15}$$

$$\boldsymbol{K}_{k+1}^{\gamma}=\boldsymbol{P}_{k+1|k}^{\gamma}\boldsymbol{H}_{k+1|k}^{\mathrm{T}}(\boldsymbol{H}_{k+1|k}\boldsymbol{P}_{k+1|k}^{\gamma}\boldsymbol{H}_{k+1|k}^{\mathrm{T}}+\bar{\boldsymbol{S}}_{k+1})^{-1}, \tag{16}$$

$$\widehat{\boldsymbol{\gamma}}_{k+1|k+1}=\widehat{\boldsymbol{\gamma}}_{k+1|k}+\boldsymbol{K}_{k+1}^{\gamma}(\boldsymbol{r}_{k+1}-\boldsymbol{H}_{k+1|k}\widehat{\boldsymbol{\gamma}}_{k+1|k}), \tag{17}$$

$$\boldsymbol{P}_{k+1|k+1}^{\gamma}=(\boldsymbol{I}-\boldsymbol{K}_{k+1}^{\gamma}\boldsymbol{H}_{k+1|k})\boldsymbol{P}_{k+1|k}^{\gamma}, \tag{18}$$

where $\rho_k^i=1$ when $\alpha_{k|k}^i>\alpha_{\max}$, $\rho_k^i=\alpha_{k|k}^i(\alpha_{\min}+\frac{\alpha_{\max}-\alpha_{\min}}{\alpha_{\max}})^{-1}$ when $\alpha_{k|k}^i\le\alpha_{\max}$.

The fault-free state subfilter is as follows:

$$\bar{\boldsymbol{x}}_{k+1|k}=\boldsymbol{A}_k\bar{\boldsymbol{x}}_{k|k}+\boldsymbol{B}_k\boldsymbol{u}_k+\boldsymbol{W}_k\widehat{\boldsymbol{\gamma}}_{k|k}-\boldsymbol{V}_{k+1|k}\widehat{\boldsymbol{\gamma}}_{k|k}, \tag{19}$$

$$\boldsymbol{P}_{k+1|k}^{x}=\boldsymbol{A}_k\boldsymbol{P}_{k|k}^{x}\boldsymbol{A}_k^{\mathrm{T}}+\boldsymbol{Q}_k^{x}+\boldsymbol{W}_k\boldsymbol{P}_{k|k}^{\gamma}\boldsymbol{W}_k^{\mathrm{T}}-\boldsymbol{V}_{k+1|k}\boldsymbol{P}_{k+1|k}^{\gamma}\boldsymbol{V}_{k+1|k}^{\mathrm{T}}, \tag{20}$$

$$\boldsymbol{K}_{k+1}^{x}=\boldsymbol{P}_{k+1|k}^{x}\boldsymbol{C}_{k+1}^{\mathrm{T}}(\boldsymbol{C}_{k+1}\boldsymbol{P}_{k+1|k}^{x}\boldsymbol{C}_{k+1}^{\mathrm{T}}+\boldsymbol{R}_{k+1})^{-1}, \tag{21}$$

$$\bar{\boldsymbol{x}}_{k+1|k+1}=\bar{\boldsymbol{x}}_{k+1|k}+\boldsymbol{K}_{k+1}^{x}(\boldsymbol{y}_{k+1}-\boldsymbol{C}_{k+1}\bar{\boldsymbol{x}}_{k+1|k}), \tag{22}$$

$$\boldsymbol{P}_{k+1|k+1}^{x}=(\boldsymbol{I}-\boldsymbol{K}_{k+1}^{x}\boldsymbol{C}_{k+1})\boldsymbol{P}_{k+1|k}^{x}, \tag{23}$$

where the residual and its covariance matrix are $\boldsymbol{r}_{k+1}=\boldsymbol{y}_{k+1}-\boldsymbol{C}_{k+1}\bar{\boldsymbol{x}}_{k+1|k}$ and $\bar{\boldsymbol{S}}_{k+1}=\boldsymbol{R}_{k+1}+\boldsymbol{C}_{k+1}\boldsymbol{P}_{k+1|k}^{x}\boldsymbol{C}_{k+1}^{\mathrm{T}}$, respectively.

The coupling equations are

$$\boldsymbol{W}_k=\boldsymbol{A}_k\boldsymbol{V}_{k|k}+\boldsymbol{E}_k, \tag{24}$$

$$\boldsymbol{V}_{k+1|k}=\boldsymbol{W}_k\boldsymbol{P}_{k|k}^{\gamma}(\boldsymbol{P}_{k+1|k}^{\gamma})^{-1}, \tag{25}$$

$$\boldsymbol{H}_{k+1|k}=\boldsymbol{C}_{k+1}\boldsymbol{V}_{k+1|k}, \tag{26}$$

$$\boldsymbol{V}_{k+1|k+1}=\boldsymbol{V}_{k+1|k}-\boldsymbol{K}_{k+1}^{x}\boldsymbol{H}_{k+1|k}. \tag{27}$$

The compensated state and covariance estimates are

$$\widehat{\boldsymbol{x}}_{k+1|k+1}=\bar{\boldsymbol{x}}_{k+1|k+1}+\boldsymbol{V}_{k+1|k+1}\widehat{\boldsymbol{\gamma}}_{k+1|k+1}, \tag{28}$$

$$\boldsymbol{P}_{k+1|k+1}=\boldsymbol{V}_{k+1|k+1}\boldsymbol{P}_{k+1|k+1}^{\gamma}\boldsymbol{V}_{k+1|k+1}^{\mathrm{T}}+\boldsymbol{P}_{k+1|k+1}^{x}. \tag{29}$$

Remark 2 The ATSKF-based FDD scheme can not only detect the actuator faults, but also provide accurate estimates of the fault amplitudes. Furthermore, it has been proven that ATSKF is an unbiased estimator, meaning that $E(\widehat{\boldsymbol{\gamma}})=\boldsymbol{\gamma}$.

3.2 Robust MRAC based controller design for trajectory tracking control

To minimize the steady-state tracking error and ensure the desired tracking performance, an integral control action is used in the controller design. Augmenting the integration of the tracking error as a system state, the dynamic model of a QUAV in Eq. (7) can be written as

$$\begin{cases}\dot{\boldsymbol{x}}(t)=(\boldsymbol{A}_0+\delta\boldsymbol{A})\boldsymbol{x}(t)+\boldsymbol{B}\boldsymbol{u}(t)+\boldsymbol{B}_{\mathrm{r}}\boldsymbol{r}(t),\\ \boldsymbol{y}(t)=\boldsymbol{C}\boldsymbol{x}(t),\end{cases} \tag{30}$$

where $\boldsymbol{x}=[\boldsymbol{x}_{\mathrm{a}}^{\mathrm{T}}\ \boldsymbol{e}_{\mathrm{I}}^{\mathrm{T}}]^{\mathrm{T}}\in\mathbb{R}^{n_{\mathrm{p}}+p+m}$ is the augmented system state, $\dot{\boldsymbol{e}}_{\mathrm{I}}=\boldsymbol{e}=\boldsymbol{r}-\boldsymbol{y}$ is the tracking error, and $\boldsymbol{r}=[x_{\mathrm{r}}\ y_{\mathrm{r}}\ z_{\mathrm{r}}\ \psi_{\mathrm{r}}]^{\mathrm{T}}$ is the reference command. $\boldsymbol{A}=\boldsymbol{A}_0+\delta\boldsymbol{A}\in\mathbb{R}^{(n_{\mathrm{p}}+p+m)\times(n_{\mathrm{p}}+p+m)}$, $\boldsymbol{B}=\begin{bmatrix}\boldsymbol{B}_{\mathrm{a}}\\ \boldsymbol{0}\end{bmatrix}\in\mathbb{R}^{(n_{\mathrm{p}}+p+m)\times p}$, $\boldsymbol{B}_{\mathrm{r}}=\begin{bmatrix}\boldsymbol{0}\\ \boldsymbol{I}\end{bmatrix}\in\mathbb{R}^{(n_{\mathrm{p}}+p+m)\times m}$, and $\boldsymbol{C}=[\boldsymbol{C}_{\mathrm{a}}\ \boldsymbol{0}]\in\mathbb{R}^{m\times(n_{\mathrm{p}}+p+m)}$ are the augmented system matrices. $\boldsymbol{A}_0=\begin{bmatrix}\boldsymbol{A}_{\mathrm{a}0}&\boldsymbol{0}\\ -\boldsymbol{C}_{\mathrm{a}}&\boldsymbol{0}\end{bmatrix}\in\mathbb{R}^{(n_{\mathrm{p}}+p+m)\times(n_{\mathrm{p}}+p+m)}$ and $\delta\boldsymbol{A}\in\mathbb{R}^{(n_{\mathrm{p}}+p+m)\times(n_{\mathrm{p}}+p+m)}$ are the augmented nominal system matrix and unknown model uncertainties, respectively.

Accordingly, the dynamic model of a QUAV with actuator faults can be described as

$$\begin{cases}\dot{\boldsymbol{x}}(t)=\boldsymbol{A}\boldsymbol{x}(t)+\boldsymbol{B}\boldsymbol{u}(t)+\boldsymbol{B}_{\mathrm{r}}\boldsymbol{r}(t)+\boldsymbol{E}\boldsymbol{f}(t),\\ \boldsymbol{y}(t)=\boldsymbol{C}\boldsymbol{x}(t),\end{cases} \tag{31}$$

where $\boldsymbol{E}=[\underline{\boldsymbol{E}}_{\mathrm{a}}^{\mathrm{T}}\ \boldsymbol{0}]^{\mathrm{T}}$.

To enable closed-loop system stability and achieve superior tracking performance, the MRAC scheme is adopted as an effective control method for state tracking (Ioannou and Sun, 1996). The control target of MRAC is to design an adaptive control law such that the actual state of the system can track the desired state of the reference model. Considering the dynamic model (30) and in the case of no model uncertainties, a reference model can be designed as

$$\dot{\boldsymbol{x}}_{\mathrm{m}}(t)=\boldsymbol{A}_{\mathrm{m}}\boldsymbol{x}_{\mathrm{m}}(t)+\boldsymbol{B}_{\mathrm{m}}\boldsymbol{r}(t), \tag{32}$$

where $\boldsymbol{x}_{\mathrm{m}}\in\mathbb{R}^{n_{\mathrm{p}}+p+m}$ is the reference state, and $\boldsymbol{A}_{\mathrm{m}}\in\mathbb{R}^{(n_{\mathrm{p}}+p+m)\times(n_{\mathrm{p}}+p+m)}$ and $\boldsymbol{B}_{\mathrm{m}}\in\mathbb{R}^{(n_{\mathrm{p}}+p+m)\times m}$ are the system matrices chosen based on the desired response characteristics.

Typically, to track the desired state $\boldsymbol{x}_{\mathrm{m}}$, the nominal system $(\boldsymbol{A}_0,\boldsymbol{B})$ and the reference model (32) are required to satisfy the state feedback for state tracking conditions (Tao et al., 2004). For the dynamic model (30) without $\delta\boldsymbol{A}$, it is assumed that an ideal control law $\boldsymbol{u}(t)=\boldsymbol{K}_1\boldsymbol{x}(t)+\boldsymbol{K}_2\boldsymbol{r}(t)$ exists such that the following matching conditions are satisfied:

$$\boldsymbol{A}_{\mathrm{m}}=\boldsymbol{A}_0+\boldsymbol{B}\boldsymbol{K}_1,\ \ \boldsymbol{B}_{\mathrm{m}}=\boldsymbol{B}\boldsymbol{K}_2+\boldsymbol{B}_r. \tag{33}$$

Because $\boldsymbol{K}_1$ and $\boldsymbol{K}_2$ are typically unknown, the adaptive control law can be defined as

$$\boldsymbol{u}(t)=\widehat{\boldsymbol{K}}_1\boldsymbol{x}(t)+\widehat{\boldsymbol{K}}_2\boldsymbol{r}(t), \tag{34}$$

where $\widehat{\boldsymbol{K}}_1\in\mathbb{R}^{p\times(n_{\mathrm{p}}+p+m)}$ and $\widehat{\boldsymbol{K}}_2\in\mathbb{R}^{p\times m}$ are the time-varying estimates of $\boldsymbol{K}_1$ and $\boldsymbol{K}_2$, respectively.

Unfortunately, when model uncertainties occur in the dynamic model (30), the abovementioned matching conditions may not be satisfied. Thus, the stability and tracking performance of QUAV cannot be guaranteed. In this case, the closed-loop system (30) can be written as

$$\begin{aligned}\dot{\boldsymbol{x}}(t)=&(\boldsymbol{A}_0+\delta\boldsymbol{A})\boldsymbol{x}(t)+\boldsymbol{B}(\widehat{\boldsymbol{K}}_1\boldsymbol{x}(t)+\widehat{\boldsymbol{K}}_2\boldsymbol{r}(t))+\boldsymbol{B}_{\mathrm{r}}\boldsymbol{r}(t)\\ =&(\boldsymbol{A}_0+\delta\boldsymbol{A}+\boldsymbol{B}\widehat{\boldsymbol{K}}_1)\boldsymbol{x}(t)+(\boldsymbol{B}\widehat{\boldsymbol{K}}_2+\boldsymbol{B}_{\mathrm{r}})\boldsymbol{r}(t)\\ =&(\boldsymbol{A}_0+\delta\boldsymbol{A}+\boldsymbol{B}\boldsymbol{K}_1)\boldsymbol{x}(t)+(\boldsymbol{B}\boldsymbol{K}_2+\boldsymbol{B}_{\mathrm{r}})\boldsymbol{r}(t)\\ &-\boldsymbol{B}\widetilde{\boldsymbol{K}}_1\boldsymbol{x}(t)-\boldsymbol{B}\widetilde{\boldsymbol{K}}_2\boldsymbol{r}(t),\end{aligned} \tag{35}$$

where $\widetilde{\boldsymbol{K}}_1=\boldsymbol{K}_1-\widehat{\boldsymbol{K}}_1$, $\widetilde{\boldsymbol{K}}_2=\boldsymbol{K}_2-\widehat{\boldsymbol{K}}_2$.

Based on the matching conditions in Eq. (33), the closed-loop system can be rewritten as

$$\begin{aligned}\dot{\boldsymbol{x}}(t)=&(\boldsymbol{A}_{\mathrm{m}}+\delta\boldsymbol{A})\boldsymbol{x}(t)+\boldsymbol{B}_{\mathrm{m}}\boldsymbol{r}(t)+\boldsymbol{B}\widetilde{\boldsymbol{K}}_1\boldsymbol{x}(t)\\ &+\boldsymbol{B}\widetilde{\boldsymbol{K}}_2\boldsymbol{r}(t).\end{aligned} \tag{36}$$

Therefore, to satisfy the matching condition, the reference model is modified as

$$\begin{aligned}\dot{\boldsymbol{x}}_{\mathrm{m}}(t)&=(\boldsymbol{A}_{\mathrm{m}}+\widehat{\delta\boldsymbol{A}})\boldsymbol{x}_{\mathrm{m}}(t)+\boldsymbol{B}_{\mathrm{m}}\boldsymbol{r}(t)\\ &=\boldsymbol{A}_{\mathrm{M}}\boldsymbol{x}_{\mathrm{m}}(t)+\boldsymbol{B}_{\mathrm{m}}\boldsymbol{r}(t),\end{aligned} \tag{37}$$

where $\boldsymbol{A}_{\mathrm{M}}=\boldsymbol{A}_{\mathrm{m}}+\widehat{\delta\boldsymbol{A}}$. $\widehat{\delta\boldsymbol{A}}$ is the estimate of $\delta\boldsymbol{A}$, which can be obtained by the RBFNN technique.

Remark 3 To ensure the satisfactory stability and performance properties of the modified reference model, a quadratic stability argument and a parameter projection algorithm are used. Owing to space limitation, they are omitted herein, and the details can be obtained from Joshi et al. (2012). In addition, the reference model is modified only if the model uncertainties $\widehat{\delta\boldsymbol{A}}$ exceed a desired threshold $\overline{\delta\boldsymbol{A}}$.

The RBFNN is a popular feedforward neural network with universal approximation capability (Park and Sandberg, 1991). A typical RBFNN contains three layers: an input layer, a hidden layer, and an output layer. Each input node is connected to all the hidden layer neurons with unity weights, while each hidden layer neuron is connected to the output node with different weights. The Gaussian functions are typically chosen as activation functions of the hidden layer. By defining $\delta\boldsymbol{A}\boldsymbol{x}$ as the output of RBFNN, the model uncertainties can be approximated as follows:

$$\boldsymbol{h}_j=\exp\left(\frac{-\|\boldsymbol{x}-\boldsymbol{c}_j\|^2}{2\boldsymbol{b}_j^2}\right), \tag{38}$$

$$\delta\boldsymbol{A}\boldsymbol{x}=\boldsymbol{W}^{\mathrm{T}}\boldsymbol{h}(\boldsymbol{x})+\boldsymbol{\varepsilon}, \tag{39}$$

$$\widehat{\delta\boldsymbol{A}}\boldsymbol{x}=\widehat{\boldsymbol{W}}^{\mathrm{T}}\boldsymbol{h}(\boldsymbol{x}), \tag{40}$$

where $\boldsymbol{x}$ denotes the input vector. $\boldsymbol{c}_j$ and $\boldsymbol{b}_j$ represent the center vector and width vector of the j^{th} neuron in the hidden layer, respectively. $\boldsymbol{h}=[\boldsymbol{h}_1\ \boldsymbol{h}_2\ \dots\ \boldsymbol{h}_n]^{\mathrm{T}}$ is the output of the hidden layer. $\boldsymbol{W}=[\boldsymbol{w}_1\ \boldsymbol{w}_2\ \dots\ \boldsymbol{w}_n]^{\mathrm{T}}$ and $\widehat{\boldsymbol{W}}=[\hat{\boldsymbol{w}}_1\ \hat{\boldsymbol{w}}_2\ \dots\ \hat{\boldsymbol{w}}_n]^{\mathrm{T}}$ are the actual and estimated weight vectors between the hidden layer and output layer, respectively. $\boldsymbol{\varepsilon}$ is the approximation error.

Theorem 1 For the dynamic model (30), the adaptive control gains are chosen as

$$\dot{\widehat{\boldsymbol{K}}}_1=-\boldsymbol{R}_1\boldsymbol{B}^{\mathrm{T}}\boldsymbol{P}\underline{\boldsymbol{e}}\boldsymbol{x}^{\mathrm{T}}, \tag{41}$$

$$\dot{\widehat{\boldsymbol{K}}}_2=-\boldsymbol{R}_2\boldsymbol{B}^{\mathrm{T}}\boldsymbol{P}\underline{\boldsymbol{e}}\boldsymbol{r}^{\mathrm{T}}, \tag{42}$$

with the parameter estimation law

$$\dot{\widehat{\boldsymbol{W}}} = \tau \underline{\boldsymbol{e}}^{\mathrm{T}} \boldsymbol{P} \boldsymbol{h}(\boldsymbol{x}), \tag{43}$$

where $\boldsymbol{R}_1 \in \mathbb{R}^{p\times p}$ and $\boldsymbol{R}_2 \in \mathbb{R}^{p\times p}$ are the positive definite matrices. τ is a scale parameter. $\underline{\boldsymbol{e}} = \boldsymbol{x}_{\mathrm{m}} - \boldsymbol{x} \in \mathbb{R}^{n_{\mathrm{p}}+p+m}$ denotes the model tracking error. $\boldsymbol{P} \in \mathbb{R}^{(n_{\mathrm{p}}+p+m)\times(n_{\mathrm{p}}+p+m)}$ represents a symmetric positive definite solution of the following Lyapunov equation:

$$\boldsymbol{A}_{\mathrm{M}}^{\mathrm{T}} \boldsymbol{P} + \boldsymbol{P} \boldsymbol{A}_{\mathrm{M}} = -\boldsymbol{Q}, \tag{44}$$

where $\boldsymbol{Q} \in \mathbb{R}^{(n_{\mathrm{p}}+p+m)\times(n_{\mathrm{p}}+p+m)}$ is an arbitrary positive definite matrix.

Proof Using Eqs. (35), (37), (39), and (40) yields

$$\begin{aligned}\dot{\underline{\boldsymbol{e}}} =& \dot{\boldsymbol{x}}_{\mathrm{m}} - \dot{\boldsymbol{x}}\\ =& (\boldsymbol{A}_{\mathrm{m}} + \delta\widehat{\boldsymbol{A}})\underline{\boldsymbol{e}} + \boldsymbol{B}\widetilde{\boldsymbol{K}}_1\boldsymbol{x} + \boldsymbol{B}\widetilde{\boldsymbol{K}}_2\boldsymbol{r}\\ &+ (\widehat{\boldsymbol{W}} - \boldsymbol{W})^{\mathrm{T}}\boldsymbol{h}(\boldsymbol{x}) - \boldsymbol{\varepsilon}\\ =& \boldsymbol{A}_{\mathrm{M}}\underline{\boldsymbol{e}} + \boldsymbol{B}\widetilde{\boldsymbol{K}}_1\boldsymbol{x} + \boldsymbol{B}\widetilde{\boldsymbol{K}}_2\boldsymbol{r} + \widetilde{\boldsymbol{W}}^{\mathrm{T}}\boldsymbol{h}(\boldsymbol{x}) - \boldsymbol{\varepsilon},\end{aligned} \tag{45}$$

where $\widetilde{\boldsymbol{W}} = \widehat{\boldsymbol{W}} - \boldsymbol{W}$.

The Lyapunov function candidate is constructed as

$$\begin{aligned}V =& \underline{\boldsymbol{e}}^{\mathrm{T}}\boldsymbol{P}\underline{\boldsymbol{e}} + \mathrm{tr}\left(\widetilde{\boldsymbol{K}}_1^{\mathrm{T}}\boldsymbol{R}_1^{-1}\widetilde{\boldsymbol{K}}_1\right)\\ &+ \mathrm{tr}\left(\widetilde{\boldsymbol{K}}_2^{\mathrm{T}}\boldsymbol{R}_2^{-1}\widetilde{\boldsymbol{K}}_2\right) + \frac{1}{\tau}\widetilde{\boldsymbol{W}}^{\mathrm{T}}\widetilde{\boldsymbol{W}}.\end{aligned} \tag{46}$$

Taking the derivative of Eq. (46) yields

$$\begin{aligned}\dot{V} =& \dot{\underline{\boldsymbol{e}}}^{\mathrm{T}}\boldsymbol{P}\underline{\boldsymbol{e}} + \underline{\boldsymbol{e}}^{\mathrm{T}}\boldsymbol{P}\dot{\underline{\boldsymbol{e}}} + \mathrm{tr}\left(\dot{\widetilde{\boldsymbol{K}}}_1^{\mathrm{T}}\boldsymbol{R}_1^{-1}\widetilde{\boldsymbol{K}}_1 + \widetilde{\boldsymbol{K}}_1^{\mathrm{T}}\boldsymbol{R}_1^{-1}\dot{\widetilde{\boldsymbol{K}}}_1\right)\\ &+ \mathrm{tr}\left(\dot{\widetilde{\boldsymbol{K}}}_2^{\mathrm{T}}\boldsymbol{R}_2^{-1}\widetilde{\boldsymbol{K}}_2 + \widetilde{\boldsymbol{K}}_2^{\mathrm{T}}\boldsymbol{R}_2^{-1}\dot{\widetilde{\boldsymbol{K}}}_2\right) + \frac{1}{\tau}\left(\dot{\widetilde{\boldsymbol{W}}}^{\mathrm{T}}\widetilde{\boldsymbol{W}}\right.\\ &\left.+\widetilde{\boldsymbol{W}}^{\mathrm{T}}\dot{\widetilde{\boldsymbol{W}}}\right)\\ =& -\underline{\boldsymbol{e}}^{\mathrm{T}}\boldsymbol{Q}\underline{\boldsymbol{e}} + 2\mathrm{tr}\left(\dot{\widetilde{\boldsymbol{K}}}_1^{\mathrm{T}}\boldsymbol{R}_1^{-1}\widetilde{\boldsymbol{K}}_1 + \boldsymbol{x}\underline{\boldsymbol{e}}^{\mathrm{T}}\boldsymbol{P}\boldsymbol{B}\widetilde{\boldsymbol{K}}_1\right)\\ &+ 2\mathrm{tr}\left(\dot{\widetilde{\boldsymbol{K}}}_2^{\mathrm{T}}\boldsymbol{R}_2^{-1}\widetilde{\boldsymbol{K}}_2 + \boldsymbol{r}\underline{\boldsymbol{e}}^{\mathrm{T}}\boldsymbol{P}\boldsymbol{B}\widetilde{\boldsymbol{K}}_2\right) - 2\underline{\boldsymbol{e}}^{\mathrm{T}}\boldsymbol{P}\boldsymbol{\varepsilon}\\ &+ 2\left(\frac{1}{\tau}\widetilde{\boldsymbol{W}}^{\mathrm{T}}\dot{\widetilde{\boldsymbol{W}}} - \underline{\boldsymbol{e}}^{\mathrm{T}}\boldsymbol{P}\widetilde{\boldsymbol{W}}^{\mathrm{T}}\boldsymbol{h}(\boldsymbol{x})\right).\end{aligned} \tag{47}$$

Substituting Eqs. (41)−(43) into Eq. (47), it is clear that

$$\dot{V} = -\underline{\boldsymbol{e}}^{\mathrm{T}}\boldsymbol{Q}\underline{\boldsymbol{e}} - 2\underline{\boldsymbol{e}}^{\mathrm{T}}\boldsymbol{P}\boldsymbol{\varepsilon} \le -\underline{\boldsymbol{e}}^{\mathrm{T}}\boldsymbol{Q}\underline{\boldsymbol{e}}. \tag{48}$$

This verifies the stability of the proposed controller, and the proof is completed.

3.3 Fault compensation mechanism

In the absence of actuator faults, the adaptive control law (34) will ensure the boundedness of the closed-loop signal and asymptotic tracking, such that $\lim_{t\to\infty}\boldsymbol{e}(t) = \boldsymbol{0}$ despite model uncertainties. However, when faults occur in actuators, the matching conditions (Eq. (33)) are violated again. In this case, the dynamic model (31) can be derived as follows:

$$\begin{aligned}\dot{\boldsymbol{x}}(t) =& \boldsymbol{A}\boldsymbol{x}(t) + \boldsymbol{B}\boldsymbol{u}(t) + \boldsymbol{B}_{\mathrm{r}}\boldsymbol{r}(t) + \boldsymbol{E}\boldsymbol{f}(t)\\ =& \boldsymbol{A}\boldsymbol{x}(t) + \boldsymbol{B}\boldsymbol{K}_1\boldsymbol{x}(t) + \boldsymbol{B}\boldsymbol{u}(t) + \boldsymbol{B}_{\mathrm{r}}\boldsymbol{r}(t) + \boldsymbol{B}\boldsymbol{K}_2\boldsymbol{r}(t)\\ &- \boldsymbol{B}\boldsymbol{K}_1\boldsymbol{x}(t) - \boldsymbol{B}\boldsymbol{K}_2\boldsymbol{r}(t) - \boldsymbol{B}\boldsymbol{f}(t)\\ =& (\boldsymbol{A}_{\mathrm{m}} + \delta\boldsymbol{A})\boldsymbol{x}(t) + \boldsymbol{B}_{\mathrm{m}}\boldsymbol{r}(t) + \boldsymbol{B}(\boldsymbol{u}(t)\\ &- \boldsymbol{K}_1\boldsymbol{x}(t) - \boldsymbol{K}_2\boldsymbol{r}(t) - \boldsymbol{f}(t)).\end{aligned} \tag{49}$$

Thus, to satisfy the matching conditions, the control input $\boldsymbol{u}(t)$ is chosen as

$$\boldsymbol{u}(t) = \boldsymbol{K}_1\boldsymbol{x}(t) + \boldsymbol{K}_2\boldsymbol{r}(t) + \boldsymbol{f}(t). \tag{50}$$

Theorem 2 For the dynamic model (31), the control input is designed as

$$\boldsymbol{u}(t) = \widehat{\boldsymbol{K}}_1\boldsymbol{x}(t) + \widehat{\boldsymbol{K}}_2\boldsymbol{r}(t) + \hat{\boldsymbol{f}}(t), \tag{51}$$

where $\widehat{\boldsymbol{K}}_1$ and $\widehat{\boldsymbol{K}}_2$ are given in Eqs. (41) and (42), respectively. $\hat{\boldsymbol{f}}(t)$ is obtained from the proposed FDD scheme. Subsequently, the QUAV system can be stable and the tracking error asymptotically goes to zero.

Proof Substituting Eq. (51) into Eq. (49), we can obtain

$$\begin{aligned}\dot{\boldsymbol{x}}(t) =& (\boldsymbol{A}_{\mathrm{m}} + \delta\boldsymbol{A})\boldsymbol{x}(t) + \boldsymbol{B}_{\mathrm{m}}\boldsymbol{r}(t)\\ &- \boldsymbol{B}(\widetilde{\boldsymbol{K}}_1\boldsymbol{x}(t) + \widetilde{\boldsymbol{K}}_2\boldsymbol{r}(t) + \tilde{\boldsymbol{f}}(t)),\end{aligned} \tag{52}$$

where $\tilde{\boldsymbol{f}}(t) = \boldsymbol{f}(t) - \hat{\boldsymbol{f}}(t)$.

According to Eqs. (37) and (52), the model tracking error is given as

$$\begin{aligned}\dot{\underline{\boldsymbol{e}}} = \dot{\boldsymbol{x}}_{\mathrm{m}} - \dot{\boldsymbol{x}} =& \boldsymbol{A}_{\mathrm{M}}\underline{\boldsymbol{e}} + \boldsymbol{B}\widetilde{\boldsymbol{K}}_1\boldsymbol{x} + \boldsymbol{B}\widetilde{\boldsymbol{K}}_2\boldsymbol{r}\\ &+ \widetilde{\boldsymbol{W}}^{\mathrm{T}}\boldsymbol{h}(\boldsymbol{x}) - \boldsymbol{\varepsilon} + \boldsymbol{B}\tilde{\boldsymbol{f}}.\end{aligned} \tag{53}$$

Consider the following Lyapunov function candidate:

$$\begin{aligned}V =& \underline{\boldsymbol{e}}^{\mathrm{T}}\boldsymbol{P}\underline{\boldsymbol{e}} + \mathrm{tr}\left(\widetilde{\boldsymbol{K}}_1^{\mathrm{T}}\boldsymbol{R}_1^{-1}\widetilde{\boldsymbol{K}}_1\right) + \mathrm{tr}\left(\widetilde{\boldsymbol{K}}_2^{\mathrm{T}}\boldsymbol{R}_2^{-1}\widetilde{\boldsymbol{K}}_2\right)\\ &+ \frac{1}{\tau}\widetilde{\boldsymbol{W}}^{\mathrm{T}}\widetilde{\boldsymbol{W}} + \tilde{\boldsymbol{f}}^{\mathrm{T}}\tilde{\boldsymbol{f}}.\end{aligned} \tag{54}$$

Subsequently, we have

$$\begin{aligned}\dot{V} =&\dot{\underline{\boldsymbol{e}}}^{\mathrm{T}}\boldsymbol{P}\underline{\boldsymbol{e}}+\underline{\boldsymbol{e}}^{\mathrm{T}}\boldsymbol{P}\dot{\underline{\boldsymbol{e}}}+\mathrm{tr}\left(\dot{\widetilde{\boldsymbol{K}}}_1^{\mathrm{T}}\boldsymbol{R}_1^{-1}\widetilde{\boldsymbol{K}}_1+\widetilde{\boldsymbol{K}}_1^{\mathrm{T}}\boldsymbol{R}_1^{-1}\dot{\widetilde{\boldsymbol{K}}}_1\right)\\&+\mathrm{tr}\left(\dot{\widetilde{\boldsymbol{K}}}_2^{\mathrm{T}}\boldsymbol{R}_2^{-1}\widetilde{\boldsymbol{K}}_2+\widetilde{\boldsymbol{K}}_2^{\mathrm{T}}\boldsymbol{R}_2^{-1}\dot{\widetilde{\boldsymbol{K}}}_2\right)+\frac{1}{\tau}\left(\dot{\widetilde{\boldsymbol{W}}}^{\mathrm{T}}\widetilde{\boldsymbol{W}}\right.\\&\left.+\widetilde{\boldsymbol{W}}^{\mathrm{T}}\dot{\widetilde{\boldsymbol{W}}}\right)+\left(\dot{\tilde{\boldsymbol{f}}}^{\mathrm{T}}\tilde{\boldsymbol{f}}+\tilde{\boldsymbol{f}}^{\mathrm{T}}\dot{\tilde{\boldsymbol{f}}}\right)\\=&-\underline{\boldsymbol{e}}^{\mathrm{T}}\boldsymbol{Q}\underline{\boldsymbol{e}}+2\mathrm{tr}\left(\dot{\widetilde{\boldsymbol{K}}}_1^{\mathrm{T}}\boldsymbol{R}_1^{-1}\widetilde{\boldsymbol{K}}_1+\boldsymbol{x}\underline{\boldsymbol{e}}^{\mathrm{T}}\boldsymbol{P}\boldsymbol{B}\widetilde{\boldsymbol{K}}_1\right)\\&+2\mathrm{tr}\left(\dot{\widetilde{\boldsymbol{K}}}_2^{\mathrm{T}}\boldsymbol{R}_2^{-1}\widetilde{\boldsymbol{K}}_2+\boldsymbol{r}\underline{\boldsymbol{e}}^{\mathrm{T}}\boldsymbol{P}\boldsymbol{B}\widetilde{\boldsymbol{K}}_2\right)+2\left(\frac{1}{\tau}\widetilde{\boldsymbol{W}}^{\mathrm{T}}\widetilde{\boldsymbol{W}}\right.\\&\left.-\underline{\boldsymbol{e}}^{\mathrm{T}}\boldsymbol{P}\,\widetilde{\boldsymbol{W}}^{\mathrm{T}}\boldsymbol{h}(\boldsymbol{x})\right)-2\underline{\boldsymbol{e}}^{\mathrm{T}}\boldsymbol{P}\boldsymbol{\varepsilon}+2\left(\tilde{\boldsymbol{f}}^{\mathrm{T}}\boldsymbol{B}^{\mathrm{T}}\boldsymbol{P}\underline{\boldsymbol{e}}\right.\\&\left.+\dot{\tilde{\boldsymbol{f}}}^{\mathrm{T}}\tilde{\boldsymbol{f}}\right).\end{aligned}\tag{55}$$

Based on Eqs. (41)−(43) and $\lim_{t\to\infty}\tilde{\boldsymbol{f}}(t)=\boldsymbol{0}$, it can be concluded that

$$\dot{V}\le-\underline{\boldsymbol{e}}^{\mathrm{T}}\boldsymbol{Q}\underline{\boldsymbol{e}}.\tag{56}$$

Therefore, the designed controller can guarantee that the closed-loop system is globally stable and that the tracking error asymptotically converges to zero.

4 Simulation results

To validate the effectiveness of the proposed AFTTCS, some numerical simulations are conducted. The dynamic model used in the study is from QBall-X4, whose nominal parameters can be referred to Zhong et al. (2018b). To effectively evaluate the trajectory tracking, fault-tolerant, and model uncertainty rejection capabilities, three different scenarios are considered in the simulations. In addition, a normal controller (designed by the conventional MRAC) is selected to compare the robust performance against model uncertainties and actuator faults.

4.1 Scenario 1: trajectory tracking with model uncertainties

The first scenario is designed to verify the robustness of the proposed approach to model uncertainties. It is assumed that 40% of model uncertainties exist in the QUAV system ($\delta\boldsymbol{A}=-40\%\boldsymbol{A}$), while the vehicle is required to track a square waveform altitude reference with different amplitudes. The simulation results are shown in Figs. 2 and 3.

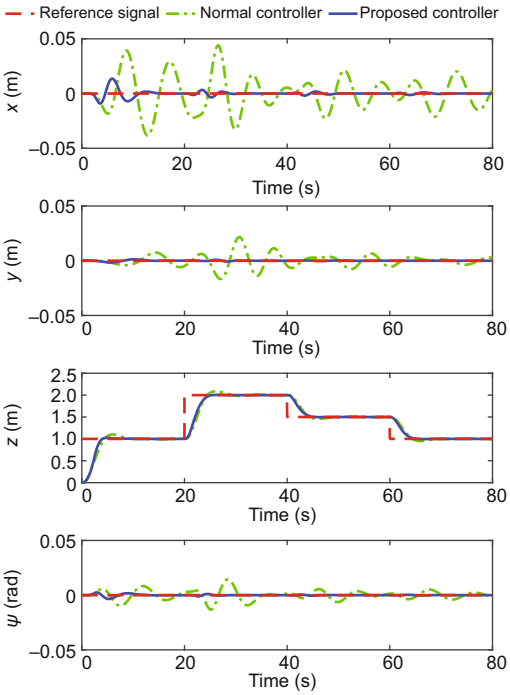

Fig. 2 Tracking performance of the different controllers in scenario 1

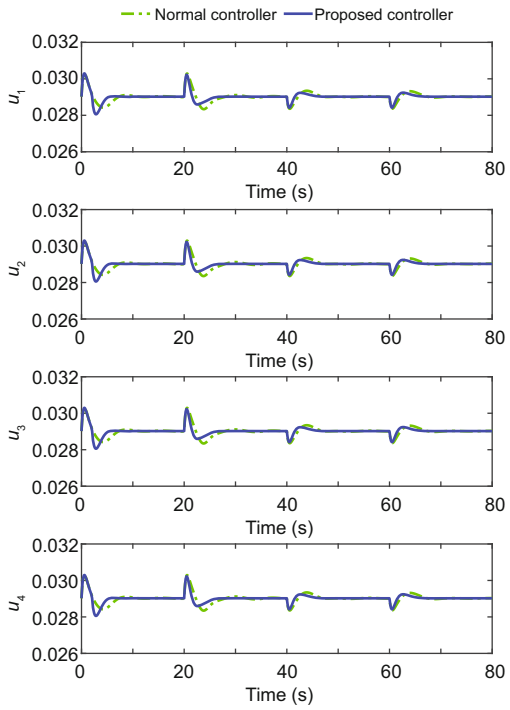

Fig. 3 Control input of the different controllers in scenario 1

As shown in Fig. 2, the tracking performance of AFTTCS is superior to that of the normal controller. The normal controller demonstrates relatively good capability in modeling uncertainties. However, when

the model uncertainties become larger, the expected tracking performance of the normal controller cannot be satisfied. For example, the actual output of x deviates from the desired reference command. In contrast, the proposed controller can still achieve a satisfactory tracking performance. Although some small glitches occur at the start of the simulation, the proposed AFTTCS can cause the QUAV to follow the desired reference trajectory after the reference model is modified in a short time. Meanwhile, as shown in Fig. 3, the control input can prove that the proposed controller is more robust than the normal controller, because the modified reference model is crucial in reducing the adverse effect of the model uncertainties.

4.2 Scenario 2: trajectory tracking with actuator faults

In the second scenario, to demonstrate the fault-tolerant capability of the proposed method, losses of 25% and 30% control effectiveness are assumed to be simultaneously injected in the first and third motors, respectively, at $t = 25$ s. Subsequently, a severe actuator fault is assumed to occur in the fourth motor with a 40% loss of control effectiveness at $t = 50$ s. The simulation results are illustrated in Figs. 4–6.

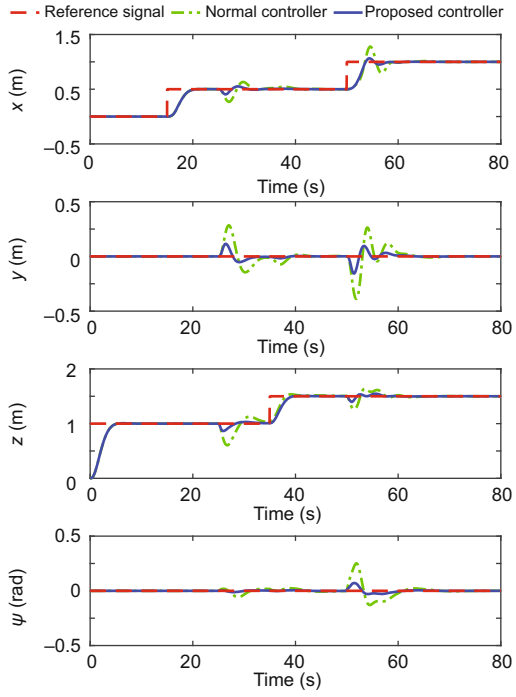

Fig. 4 Tracking performance of the different controllers in scenario 2

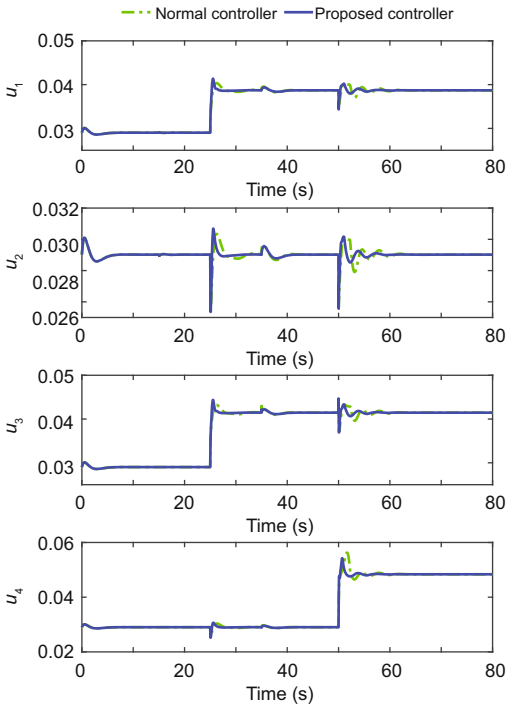

Fig. 5 Control input of the different controllers in scenario 2

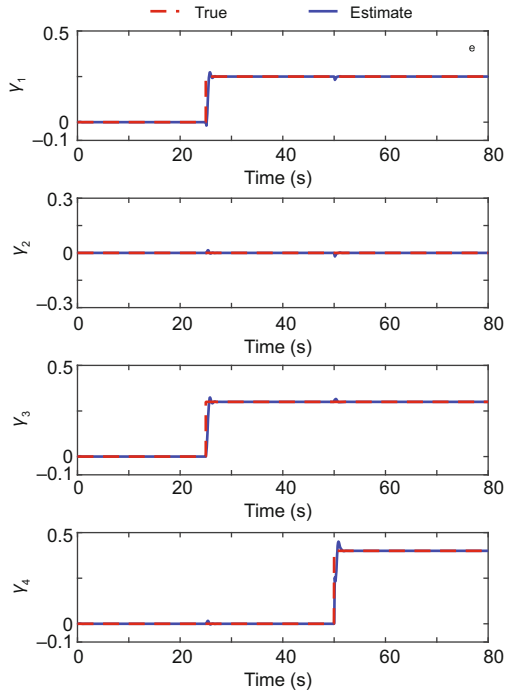

Fig. 6 Fault estimation results in scenario 2

As shown in Fig. 4, the proposed controller provides a more satisfactory tracking performance than the normal controller after the occurrence of the actuator faults. When the actuators operate well, the proposed and normal controllers exhibit the

same tracking performance. However, when actuator faults occur, despite both of them being capable of driving the QUAV back to the desired trajectory after a transient period, the proposed AFTTCS can stabilize the system with a smaller overshoot and less settling time than the normal controller. Specifically, the overshoot in the x response of the normal controller is almost five times that of the proposed controller after a 40% loss in control effectiveness is imposed in the fourth motor. As shown in Fig. 5, the proposed controller can achieve a faster actuator action than the normal controller to counteract the adverse effect of the actuator faults. This can be attributed to the fault compensation mechanism. Moreover, it is shown in Fig. 6 that the FDD scheme can provide a fast and accurate estimation of the LOE factor. Even though two actuator faults occur simultaneously, the FDD scheme can distinguish them and estimate the real value of each LOE factor.

4.3 Scenario 3: trajectory tracking with model uncertainties and actuator faults

To further demonstrate the effectiveness of the proposed AFTTCS, both model uncertainties and actuator faults are considered in the third scenario. Further, 30% of model uncertainties are assumed to be subtracted in system matrix $\boldsymbol{A}$, thus indicating that $\delta\boldsymbol{A} = -30\%\boldsymbol{A}$. Meanwhile, it is assumed that a 20% loss in control effectiveness in the first motor and a 30% loss in control effectiveness in the fourth motor occur at $t = 15$ s and $t = 40$ s, respectively. Subsequently, the first actuator fault is assumed to become worse from 20% to 36% at $t = 60$ s. The simulation results are displayed in Figs. 7–9.

As shown in Fig. 7, the tracking performance of the proposed AFTTCS under more complicated situations is still satisfactory. The proposed controller enables the vehicle to track the reference input accurately even in the presence of model uncertainties and actuator faults. However, without a modified reference model and a fault compensation mechanism, the performance of the normal controller becomes unacceptable with a high overshoot. It is obvious that the tracking error of the normal controller is larger than that of the proposed AFTTCS. As shown in Fig. 8, more appropriate control inputs are produced by the proposed controller in comparison with the normal controller, thus contributing to mitigating the negative impacts of model uncertainties

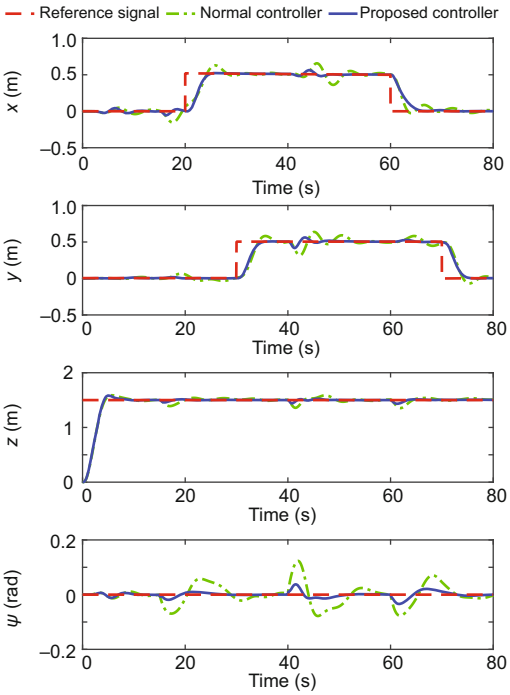

Fig. 7 Tracking performance of the different controllers in scenario 3

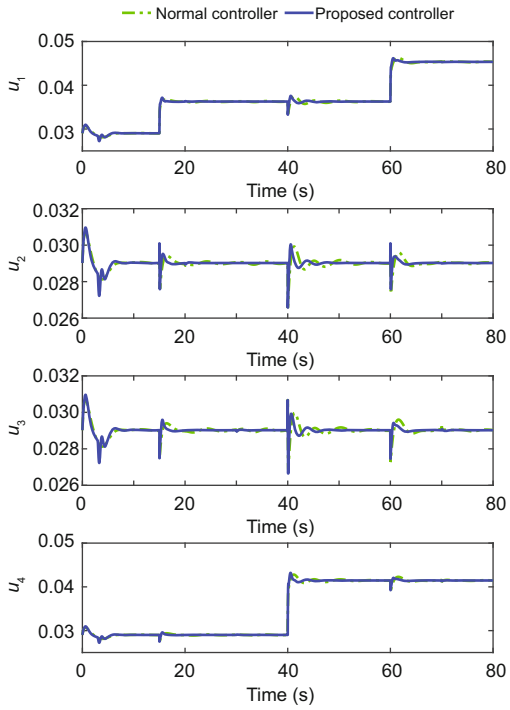

Fig. 8 Control input of the different controllers in scenario 3

and actuator faults. From Fig. 9, it is evident that the FDD scheme still achieves superior fault estimation performance despite model uncertainties. It is noteworthy that some missed detections that occur

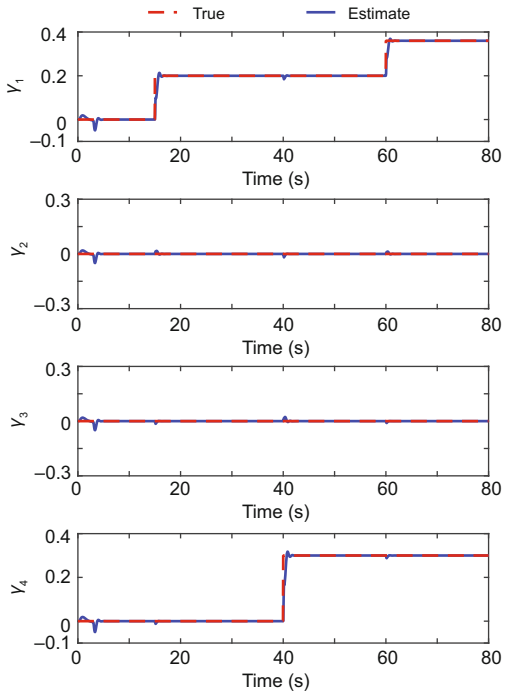

Fig. 9 Fault estimation results in scenario 3

in the beginning of the simulation are induced by model uncertainties. Using the RBFNN technique, the system matrix is modified and the estimation performance of the FDD scheme is improved.

5 Conclusions

A high-performance AFTTCS was designed for a QUAV with model uncertainties and actuator faults in this study. Fundamentally, AFTTCS used the MRAC scheme. An integral control action was first integrated into AFTTCS to minimize the steady-state tracking error. Subsequently, an RBFNN method was employed to approximate the unknown model uncertainties to modify the mismatched reference model. Using an ATSKF-based FDD scheme, a fault compensating mechanism was incorporated into AFTTCS and effectively counteracted the adverse effects of the actuator faults. The stability of AFTTCS was proven through the Lyapunov stability theory. Finally, the simulation results demonstrated that AFTTCS could achieve a satisfactory tracking performance even in the presence of larger model uncertainties and severe actuator faults. In future work, the proposed AFTTCS will be validated on a real QBall-X4 testbed.

References

Avram RC, Zhang XD, Muse J, 2018. Nonlinear adaptive fault-tolerant quadrotor altitude and attitude tracking with multiple actuator faults. *Trans Contr Syst Technol*, 26(2):701-707. https://doi.org/10.1109/TCST.2017.2670522

Chen FY, Zhang KK, Wang Z, et al., 2015. Trajectory tracking of a quadrotor with unknown parameters and its fault-tolerant control via sliding mode fault observer. *Proc Inst Mech Eng Part I J Syst Contr Eng*, 229(4):279-292. https://doi.org/10.1177/0959651814566040

Chen FY, Jiang RQ, Zhang KK, et al., 2016. Robust backstepping sliding-mode control and observer-based fault estimation for a quadrotor UAV. *IEEE Trans Ind Electron*, 63(8):5044-5056. https://doi.org/10.1109/TIE.2016.2552151

Cheng E, 2015. Aerial photography and videography using drones. In: Johnson K (Ed.), Aerial Photograph Techniques. Peachpit Press, San Francisco.

Dydek ZT, Annaswamy AM, Lavretsky E, 2013. Adaptive control of quadrotor UAVs: a design trade study with flight evaluations. *IEEE Trans Contr Syst Technol*, 21(4):1400-1406. https://doi.org/10.1109/TCST.2012.2200104

Hao W, Xian B, 2017. Nonlinear adaptive fault-tolerant control for a quadrotor UAV based on immersion and invariance methodology. *Nonl Dynam*, 90(4):2813-2826. https://doi.org/10.1007/s11071-017-3842-1

Ioannou PA, Sun J, 1996. Robust Adaptive Control. Prentice-Hall, Upper Saddle River, NJ, USA.

Joshi SM, Patre P, Tao G, 2012. Adaptive control of systems with actuator failures using an adaptive reference model. *J Guid Contr Dynam*, 35(3):938-949. https://doi.org/10.2514/1.54332

Kayacan E, Maslim R, 2017. Type-2 fuzzy logic trajectory tracking control of quadrotor VTOL aircraft with elliptic membership functions. *IEEE/ASME Trans Mech*, 22(1):339-348. https://doi.org/10.1109/TMECH.2016.2614672

Liu ZX, Yuan C, Zhang YM, et al., 2016. A learning-based fault tolerant tracking control of an unmanned quadrotor helicopter. *J Intell Rob Syst*, 84(1-4):145-162. https://doi.org/10.1007/s10846-015-0293-0

Liu ZX, Yuan C, Yu X, et al., 2017. Retrofit fault-tolerant tracking control design of an unmanned quadrotor helicopter considering actuator dynamics. *Int J Robust Nonl Contr*, in press. https://doi.org/10.1002/rnc.3889

Mallavalli S, Fekih A, 2018. A fault tolerant tracking control for a quadrotor UAV subject to simultaneous actuator faults and exogenous disturbances. *Int J Contr*, in press. https://doi.org/10.1080/00207179.2018.1484173

Murray CC, Chu AG, 2015. The flying sidekick traveling salesman problem: optimization of drone-assisted parcel delivery. *Transp Res Part C Emerg Technol*, 54:86-109. https://doi.org/10.1016/j.trc.2015.03.005

Park J, Sandberg IW, 1991. Universal approximation using radial-basis-function networks. *Neur Comput*, 3(2):246-257. https://doi.org/10.1162/neco.1991.3.2.246

Ríos H, Falcòn R, González OA, et al., 2018. Continuous sliding-modes control strategies for quad-rotor robust tracking: real-time application. *IEEE Trans Ind Electron*, 66(2):1264-1272. https://doi.org/10.1109/TIE.2018.2831191

Tao G, Chen SH, Tang XD, et al., 2004. State feedback designs for state tracking. In: Tao G, Chen SH, Tang XD, et al. (Eds.), Adaptive Control of Systems with Actuator Failures. Springer, London, p.15-54. https://doi.org/10.1007/978-1-4471-3758-0_2

Wang B, Ghamry KA, Zhang YM, 2016. Trajectory tracking and attitude control of an unmanned quadrotor helicopter considering actuator dynamics. 35th Chinese Control Conf, p.10795-10800. https://doi.org/10.1109/ChiCC.2016.7555068

Wu EN, Zhang YM, Zhou KM, 2000. Detection, estimation, and accommodation of loss of control effectiveness. *Int J Adapt Contr Signal Process*, 14(7):775-795. https://doi.org/10.1002/1099-1115(200011)14:7<775::AID-ACS621>3.0.CO;2-4

Xiong JJ, Zhang GB, 2017. Global fast dynamic terminal sliding mode control for a quadrotor UAV. *ISA Trans*, 66:233-240. https://doi.org/10.1016/j.isatra.2016.09.019

Xu R, Ozguner U, 2006. Sliding mode control of a quadrotor helicopter. 45th IEEE Conf on Decision and Control, p.4957-4962. https://doi.org/10.1109/CDC.2006.377588

Xu ZW, Nian XH, Wang HB, et al., 2017. Robust guaranteed cost tracking control of quadrotor UAV with uncertainties. *ISA Trans*, 69:157-165. https://doi.org/10.1016/j.isatra.2017.03.023

Yacef F, Bouhali O, Hamerlain M, et al., 2016. Observer-based adaptive fuzzy backstepping tracking control of quadrotor unmanned aerial vehicle powered by Li-ion batter. *J Intell Robot Syst*, 84(1-4):179-197. https://doi.org/10.1007/s10846-016-0345-0

Yuan C, Liu ZX, Zhang YM, 2015. UAV-based forest fire detection and tracking using image processing technique. Int Conf on Unmanned Aircraft Systems p.639-643. https://doi.org/10.1109/ICUAS.2017.7991306

Zhang CH, Kovacs JM, 2012. The application of small unmanned aerial systems for precision agriculture: a review. *Prec Agric*, 13(6):693-712. https://doi.org/10.1007/s11119-012-9274-5

Zhang YM, Jiang J, 2002. Active fault-tolerant control system against partial actuator failures. *IEE Proc Contr Theory Appl*, 149(1):95-104. https://doi.org/10.1049/ip-cta:20020110

Zhang YM, Jiang J, 2008. Bibliographical review on reconfigurable fault-tolerant control systems. *Ann Rev Contr*, 32(2):229-252. https://doi.org/10.1016/j.arcontrol.2008.03.008

Zhong YJ, Zhang W, Zhang YM, 2018a. Active fault-tolerant tracking control of a quadrotor UAV. Int Conf on Sensing, Diagnostics, Prognostics, and Control.

Zhong YJ, Zhang YM, Zhang W, et al., 2018b. Robust actuator fault detection and diagnosis for a quadrotor UAV with external disturbances. *IEEE Access*, 6:48169-48180. https://doi.org/10.1109/ACCESS.2018.2867574

Zou Y, Zhu B, 2017. Adaptive trajectory tracking controller for quadrotor systems subject to parametric uncertainties. *J Frankl Inst*, 354(15):6724-6746. https://doi.org/10.1016/j.jfranklin.2017.08.027